2012

Improved hydrogen storage properties of MgH2 doped with chlorides of transition metals Hf and Fe

M Ismail Ismail
University of Malaysia, mi300@uow.edu.au

Yue Zhao
University of Wollongong, yue@uow.edu.au

Xuebin Yu
Fudan University, University Of Wollongong, xyu@uow.edu.au

S X. Dou
University of Wollongong, shi@uow.edu.au

Publication Details

Ismail, M., Zhao, Y., Yu, X. & Dou, S. X. (2012). Improved hydrogen storage properties of MgH2 doped with chlorides of transition metals Hf and Fe. Energy Education Science and Technology Part A: Energy Science and Research, 30 (SPEC.ISS.1), 107-122.

Improved hydrogen storage properties of MgH2 doped with chlorides of transition metals Hf and Fe

Abstract
The effects of HfCl4 and FeCl3 addition on the de/rehydrogenation properties of MgH2 were investigated. Both HfCl4 and FeCl3-doped MgH2 samples started to released hydrogen at about 270 °C, a decreased of about 70 °C and about 140 °C compared to as-milled and as-received MgH2, respectively. In terms of the desorption kinetics, the HfCl4-doped MgH2 sample showed significant improvement, with 6.0 wt.% hydrogen released within 10 min at 300 °C, while the FeCl3-doped MgH2 and undoped MgH2 samples released 3.5 and 0.2 wt.% hydrogen, respectively, under the same conditions. In terms of the absorption kinetics, 5.5 wt.% hydrogen was charged at 300 °C under 3.0 MPa hydrogen in 1 minute for the HfCl4-doped MgH2 sample, while 4.8 wt.% was absorbed by the FeCl3-doped MgH2 sample, compared to just 3.0 wt.% hydrogen for the undoped MgH2 sample under the same conditions. From the Arrhenius plot based on isothermal dehydrogenation kinetics at different temperatures, the apparent activation energy of as-milled MgH2 is calculated to be 166 kJ/mol, and this value is reduced by 64 and 36 kJ/mol after doping with HfCl4 and FeCl3, respectively. A cycling study of dehydrogenation at 300 °C shows that the hydrogen capacity of the HfCl4-doped MgH2 sample was maintained at about 6 wt.% after 10 cycles. Based on the X-ray diffraction, Fourier transform infrared spectroscopy, and X-ray photoelectron spectroscopy examinations, we believe that the significant improvement of MgH2 sorption properties in the doped samples is due to the catalytic effects of in-situ generated metal species and MgCl2 that were formed during the dehydrogenation process.

Keywords
storage, hydrogen, mgh2, doped, fe, improved, properties, chlorides, transition, metals, hf

Disciplines
Engineering | Science and Technology Studies

Publication Details
Ismail, M., Zhao, Y., Yu, X. & Dou, S. X. (2012). Improved hydrogen storage properties of MgH2 doped with chlorides of transition metals Hf and Fe. Energy Education Science and Technology Part A: Energy Science and Research, 30 (SPEC.ISS.1), 107-122.

Improved hydrogen storage properties of MgH_2 doped with chlorides of transition metals Hf and Fe

M. Ismail[1,2,*], Y. Zhao[1,3], X. B. Yu[1,4], S. X. Dou[1]

[1]*University of Wollongong, Institute for Superconducting and Electronic Materials, Wollongong, NSW, Australia*
[2]*Universiti Malaysia Terengganu, Department of Physical Sciences, Faculty of Science and Technology, Terengganu, Kuala Terengganu, Malaysia*
[3]*University of Wollongong, School of Mechanical, Materials and Mechatronics Engineering, NSW, Australia*
[4]*Fudan University, Department of Materials Science, Shanghai, China*

Abstract

The effects of $HfCl_4$ and $FeCl_3$ addition on the de/rehydrogenation properties of MgH_2 were investigated. Both $HfCl_4$ and $FeCl_3$-doped MgH_2 samples started to released hydrogen at about 270 °C, a decreased of about 70 °C and about 140 °C compared to as-milled and as-received MgH_2, respectively. In terms of the desorption kinetics, the $HfCl_4$-doped MgH_2 sample showed significant improvement, with 6.0 wt.% hydrogen released within 10 min at 300 °C, while the $FeCl_3$-doped MgH_2 and undoped MgH_2 samples released 3.5 and 0.2 wt.% hydrogen, respectively, under the same conditions. In terms of the absorption kinetics, 5.5 wt.% hydrogen was charged at 300 °C under 3.0 MPa hydrogen in 1 minute for the $HfCl_4$-doped MgH_2 sample, while 4.8 wt.% was absorbed by the $FeCl_3$-doped MgH_2 sample, compared to just 3.0 wt.% hydrogen for the undoped MgH_2 sample under the same conditions. From the Arrhenius plot based on isothermal dehydrogenation kinetics at different temperatures, the apparent activation energy of as-milled MgH_2 is calculated to be 166 kJ/mol, and this value is reduced by 64 and 36 kJ/mol after doping with $HfCl_4$ and $FeCl_3$, respectively. A cycling study of dehydrogenation at 300 ºC shows that the hydrogen capacity of the $HfCl_4$-doped MgH_2 sample was maintained at about 6 wt.% after 10 cycles. Based on the X-ray diffraction, Fourier transform infrared spectroscopy, and X-ray photoelectron spectroscopy examinations, we believe that the significant improvement of MgH_2 sorption properties in the doped samples is due to the catalytic effects of in-situ generated metal species and $MgCl_2$ that were formed during the dehydrogenation process.

Keywords: MgH_2; $HfCl_4$; $FeCl_3$; Catalytic effect

[*]Corresponding author. Tel: +609-668-3487; fax: +609-669-4660.
E-mail address: mohammadismail@umt.edu.my (M. Ismail).

1. Introduction

Safety and cost are the two major technical challenges for the commercialization of hydrogen storage in pressurized gas and cryogenic liquid forms. Apart from the two forms mentioned above, solid-state hydrogen storage has been an attractive option due to its high gravimetric hydrogen capacity and favourable safety considerations. Solid-state hydrogen storage materials can be dividing into two categories, which is *physically bound hydrogen*; where the hydrogen gas is physisorbed to a high surface area substrate (exterior or interior) such as carbon nanotubes [1, 2], and *chemically bound hydrogen*; where the hydrogen has formed a chemical compounds with the substrate (e.g. metal hydrides [3,4] and complex hydrides [4-7]) and the hydrogen is desorbed through a thermal decomposition. Among them, metal hydride, especially MgH_2, exhibits promising potential as an energy carrier due to the high energy density (7.6 wt.% for MgH_2), with the added advantages of low cost and superior reversibility [8-13]. Nevertheless, its high decomposition temperature and slow desorption/absorption kinetics are two problems that limit the use of MgH_2 as a hydrogen storage material [14, 15]. Extensive efforts have been made to overcome these problems, including the introduction of catalysts into MgH_2. Various catalysts have been doped into MgH_2 by mechanical milling. These include metals [16-18], metal oxides [19, 20], transition metal halides [21-26], carbon materials [27, 28], nanosized alloys [29, 30], and combinations of carbon materials and transition metals, transition metal halides, and $Ti_{0.4}Mn_{0.22}Cr_{0.1}V_{0.28}$, with this last combination termed BCC composite because of its body centred cubic structure [31-33].

Many studies have shown that the transition-metal compounds showed high effective catalysis due to the high affinity of transition-metal cations toward hydrogen [17, 34-36]. In addition, transition metal fluorides, such as TiF_3 and NbF_5, have been introduced into MgH_2 to enhance its kinetics [21, 22, 25, 37]. It was claimed that both metal and fluorine anions contribute to the kinetic enhancement of MgH_2. As a source of both transition metal and halogen anions, transition metal halides are attractive for use as an additive to prepare an Mg-based hydrogen storage system.

In this work, $FeCl_3$ and $HfCl_4$, with the aim of combining the functions of both transition metal cations and chlorine anions, will be introduced to prepare a MgH_2–metal chloride system. Samples were analysed by Sieverts type pressure-composition-temperature (PCT) apparatus, differential scanning calorimetry (DSC), X-ray diffraction (XRD), Fourier transform infrared spectroscopy (FTIR), and X-ray photoelectron spectroscopy (XPS). The possible catalysis mechanism of the two dopants is then discussed.

2. Experimental details

Pure MgH_2 (hydrogen storage grade), $HfCl_4$ (98% purity), $FeCl_3$ (reagent grade, 97%), and $MgCl_2$ (anhydrous, $\geq$ 98%) were purchased from Sigma-Aldrich. Hafnium powder (-325 mesh, 99.6%) and Iron powder (-200 mesh, 99+% (metal basis)) were purchased from Alfa Aesar. All materials were used as received with no further purification. The MgH_2 and additives were respectively loaded into a sealed stainless steel vial together with hardened stainless steel balls in an argon atmosphere MBraun Unilab glove box. The ratio of the weight of the balls to the weight of powder was 40:1. The samples were then milled in a planetary ball mill (QM-3SP2) for 1 h, by first milling for 0.5 h, resting for 6 min, and then milling for another 0.5 h in a different direction at the rate of 400 rpm.

The experiments on de/re-hydrogenation were performed in a Sieverts-type pressure-composition-temperature (PCT) apparatus (Advanced Materials Corporation). The sample was loaded into a sample vessel in the glove box. For the temperature programmed desorption (TPD) measurements, all the samples were heated in a vacuum chamber, and the amount of desorbed hydrogen was measured to determine the lowest decomposition temperature. The heating rate for the TPD experiment was 5 °C/min, and samples were heated from room temperature to 450ºC. The de/re-hydrogenation kinetics measurements were conducted at the desired temperature with initial hydrogen pressures of 0.001 MPa and 3.0 MPa, respectively.

XRD analysis was performed using a GBC MMA X-ray diffractometer with Cu K_α radiation. θ-2θ scans were carried out over diffraction angles from 20° to 80° with a speed of 2.00 °/min. Before the measurement, a small amount of sample was spread uniformly on the sample holder, which was wrapped with plastic wrap to prevent oxidation.

Differential scanning calorimetry (DSC) analysis of the dehydrogenation process was carried out on a Mettler Toledo TGA/DSC 1. The sample was loaded into an alumina crucible in the glove box. The crucible was then placed in a sealed glass bottle in order to prevent oxidation during transportation from the glove box to the DSC apparatus. An empty alumina crucible was used for reference. The samples were heated from room temperature to 500 °C under an argon flow of 30 ml/min, and the heating rate was 15 °C/min.

Fourier transformation infrared (FTIR) spectroscopy analyses were carried out using a Shimadzu IRPrestige-21 model equipped with a KBr beamsplitter and a deuterated\ L-alanine triglycine sulfide (DLATGS) detector. Samples were mixed uniformly with potassium bromide (KBr) powder with an agate mortar and pestle, and then put into the sample holder. KBr background spectra were recorded before analysis of the samples. 40 scans were carried out between 400 and 1600 cm^{-1}, with a spectral resolution of 4 cm^{-1}.

X-ray photoelectron spectroscopy (XPS) were obtained using a SPECS PHOIBOS 100 analyser installed in a high-vacuum chamber with the base pressure below 10^{-8} mbar; X-ray excitation was provided by Al Kα radiation with photon energy $h\nu$ = 1486.6 eV at a high voltage of 12 kV and a power of 120 W. The XPS binding energy spectra were recorded at the pass energy of 20 eV in the fixed analyser transmission mode, and the XPS spectra of the doped samples were collected after bombardment of the sample using an Ar ion source with ion energy of 5 keV. Samples were prepared inside an Ar glove box, by dusting powders onto an adhesive carbon tape. The samples were then placed in a sealed container in order to reduce oxidation during transportation from the glove box to the XPS apparatus. Analysis of the XPS data was carried out using a commercial CasaXPS2.3.15 software package. The background was corrected using the linear approximation.

3. Results and discussion

Fig. 1 shows the temperature-programmed desorption (TPD) patterns for the dehydrogenation of as-received MgH_2, as-milled MgH_2, MgH_2 + 10 wt.% $HfCl_4$, and MgH_2 + 10 wt.% $FeCl_3$. The as-received MgH_2 starts to release hydrogen at about 410 °C, with a total dehydrogenation capacity of 7.0 wt.% H_2 by 430 °C. After milling, the onset desorption temperature of MgH_2 was reduced to about 340 °C, indicating that the milling process also influences the onset desorption temperature of MgH_2, as reported by Huot et al. [38]. After doping with $HfCl_4$ and $FeCl_3$, the onset desorption temperature of MgH_2 decreased dramatically. Both of the doped samples start to release hydrogen at about 270 °C, a decrease of about 70 °C and about 140 °C compared with the

as-milled and as-received MgH_2, respectively. However, the $HfCl_4$-doped MgH_2 sample showed faster desorption rates than the $FeCl_3$-doped MgH_2 sample.

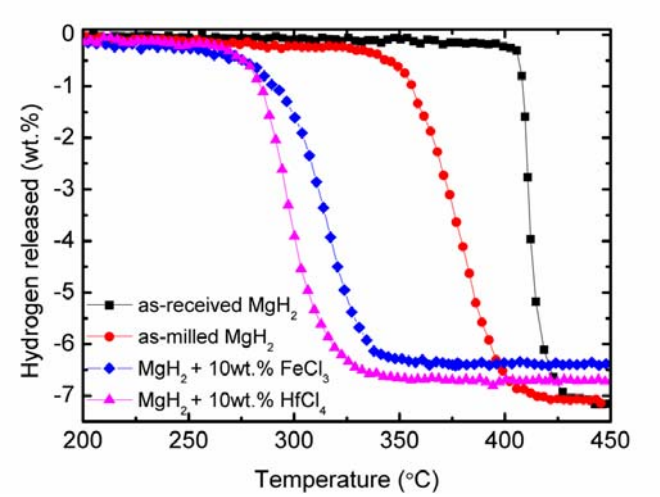

Fig. 1. Temperature-programmed desorption (TPD) patterns for the dehydrogenation of as-received MgH_2, as-milled MgH_2, MgH_2 + 10 wt.% $FeCl_3$, and MgH_2 + 10 wt.% $HfCl_4$.

The thermal properties of the as-milled MgH_2, and the $HfCl_4$- and $FeCl_3$-doped MgH_2 samples were further investigated by DSC, as shown in Fig. 2. The as-milled MgH_2 starts to release hydrogen at about 380 °C. After doping with $HfCl_4$ or $FeCl_3$, MgH_2 starts to release hydrogen at about 310 °C, which represents a reduction of about 70 °C compared to the as-milled MgH_2. This result is comparable with the results of the PCT measurements (Fig. 1). Furthermore, it can be seen that the onset decomposition temperatures of the samples in DSC are slightly higher than in the TPD (Fig. 1). These differences may result from the fact that the dehydrogenation was conducted under different heating rates and different heating atmospheres in the two types of measurements.

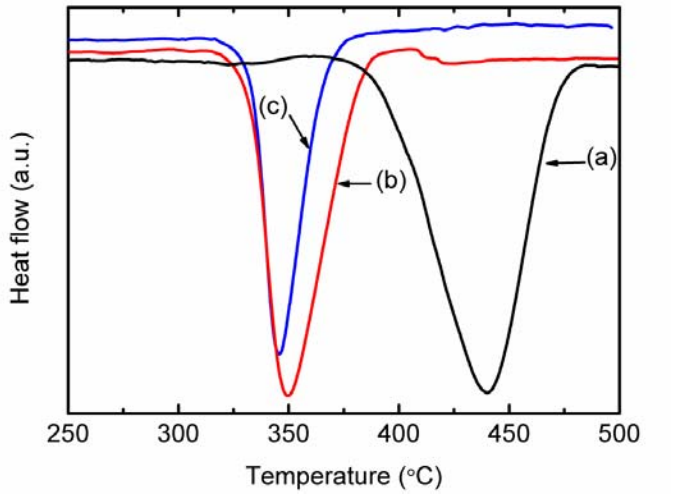

Fig. 2. DSC traces of (a) as-milled MgH_2, (b) MgH_2 + 10 wt.% $FeCl_3$, and (c) MgH_2 + 10 wt.% $HfCl_4$. Heating rate: 15 °C min^{-1}, argon flow: 30 ml/min.

In order to investigate the performance of the hydrogen desorption kinetics, the hydrogen desorption capacity at constant temperature was measured. Fig. 3a and 3b presents typical hydrogen desorption curves at 300 °C and 280 °C. It is clear that doping MgH_2 with $HfCl_4$ significantly improves the desorption kinetics. The $HfCl_4$-doped MgH_2 sample can release about 5.2 wt.% hydrogen in 5 min at 300 °C, while the $FeCl_3$-doped MgH_2 and the undoped MgH_2 samples released about 1.5 wt.% and 0.2 wt.% hydrogen, respectively, under the same conditions. A further desorption kinetics study at 280 °C shows that the $HfCl_4$-doped MgH_2 sample released

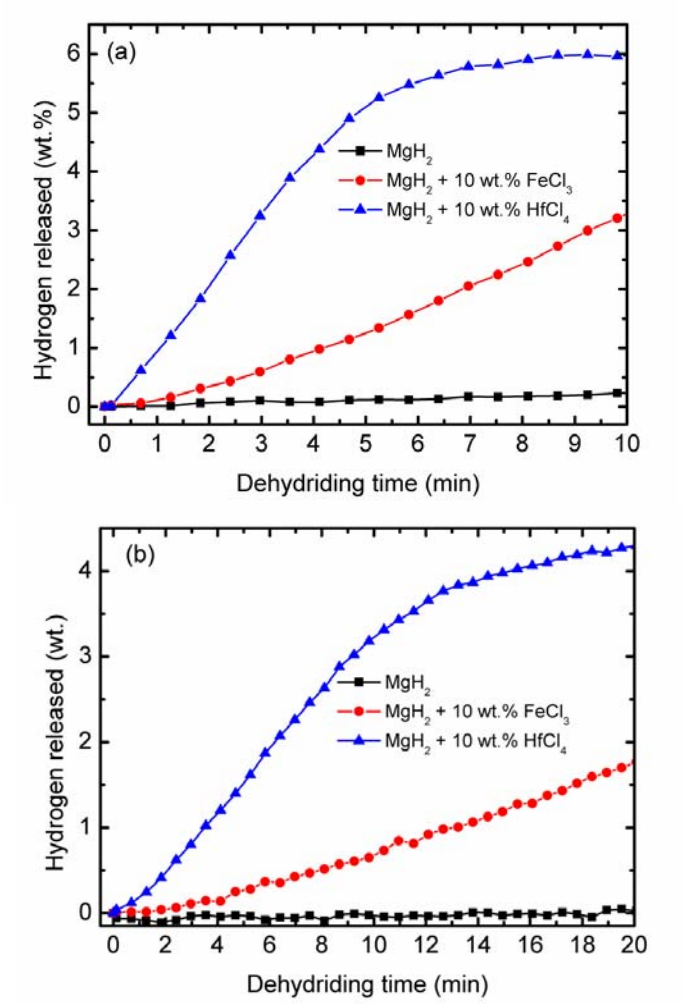

Fig. 3. Desorption kinetics measurements of MgH_2, MgH_2 + 10 wt.% $FeCl_3$, and MgH_2 + 10 wt.% $HfCl_4$ at (a) 300 °C and (b) 280 °C under vacuum.

about 4.3 wt.% hydrogen within 20 min and the $FeCl_3$-doped MgH_2 sample released about 2.7 wt.%, but no hydrogen release from the pure MgH_2 was observed. This result indicates that doping with $HfCl_4$ results in significant improvement in desorption kinetics for MgH_2 compared with $FeCl_3$ doping. This kinetic enhancement is related to the energy barrier for H_2 release from MgH_2. In order to determine the effects of $FeCl_3$ and $HfCl_4$ addition on the activation energy of MgH_2, the Arrhenius equation was employed. From the Arrhenius equation, the isothermal kinetics depends on the heating temperature and can be expressed as

$$k = k_o \exp(-E_A/RT) \quad (1)$$

where k is the rate of dehydrogenation, k_o is a temperature-independent coefficient, E_A is the apparent activation energy for hydride decomposition, R is the gas constant, and T is the absolute temperature. As shown in Fig. 4, by plotting ln(k) vs. 1/T, the apparent activation energy, E_A, for H_2 release from the as-milled MgH_2 sample, the $FeCl_3$-doped MgH_2 sample, and the $HfCl_4$-doped MgH_2 sample can be estimated. From the calculation, the apparent activation energy, E_A, for the as-milled MgH_2 is 166 kJ/mol, which is comparable to the values of 168 kJ/mol and 162 kJ/mol obtained by DSC (Kissinger method), as reported in our previous papers [39,40]. This value can be lowered by 36 kJ/mol and 62 kJ/mol after doping with $FeCl_3$ and $HfCl_4$. (E_A = 130 kJ/mol for the $FeCl_3$-doped MgH_2, and E_A = 102 kJ/mol for the $HfCl_4$-doped MgH_2.) Thus, the decreased activation energy indicates that the desorption kinetics of the MgH_2 is significantly improved.

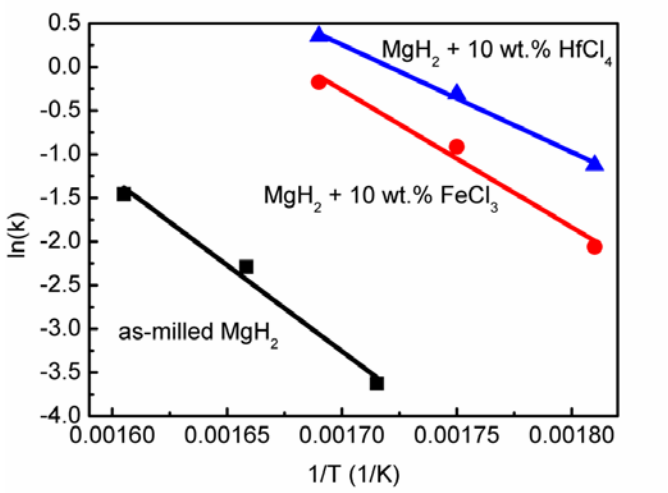

Fig. 4. Arrhenius plots of ln(k) vs. 1/T for as-milled MgH_2, MgH_2 + 10 wt.% $FeCl_3$, and MgH_2 + 10 wt.% $HfCl_4$.

Fig. 5(a) and (b) shows the absorption kinetics measurements at two different temperatures for the $HfCl_4$ and the $FeCl_3$-doped MgH_2. For comparison, the MgH_2 is also included in this figure. The samples were soaked at two constant temperatures (280 and 300 °C) under 3 MPa hydrogen pressure. The doped samples show a significant improvement with respect to absorption kinetics. The hydrogen absorbed by the $HfCl_4$-doped MgH_2 sample at 300 °C reached 5.3 wt.% within 1 min, and a hydrogen absorption capacity of 4.6 wt.% was reached by the $FeCl_3$-doped MgH_2 sample at the same time. In contrast, the undoped MgH_2 sample just absorbed 2.8 wt.% hydrogen over the same time. Furthermore, the $HfCl_4$ and $FeCl_3$-doped MgH_2 samples can absorb 4.5 and 4.0 wt.% hydrogen at 280°C within 1 min, respectively, which is higher than for the MgH_2 at 300 °C.

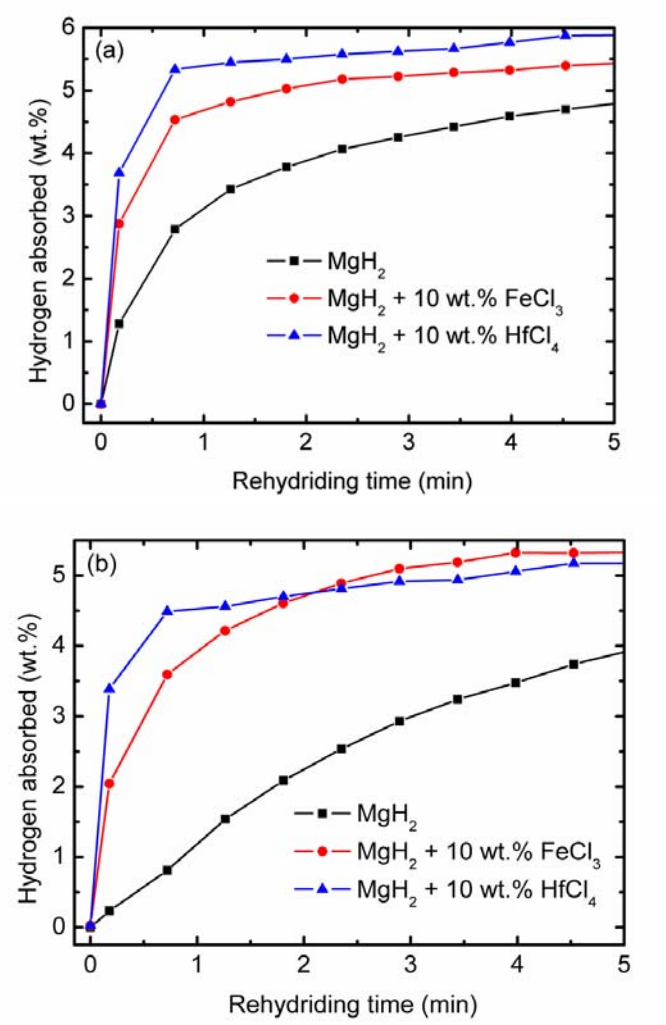

Fig. 5. Absorption kinetics measurement of MgH_2, MgH_2 + 10 wt.% $FeCl_3$, and MgH_2 + 10 wt.% $HfCl_4$ at (a) 300 °C and (b) 280 °C under 3 MPa hydrogen pressure.

Since $HfCl_4$ shows the best catalytic effects on the hydrogen absorption/desorption kinetics of MgH_2, the cycling performance of the $HfCl_4$-doped MgH_2 sample was further characterized. The cycling performance of the MgH_2 + 10 wt.% $HfCl_4$ sample at 300 °C after rehydrogenation at 300 °C under 3 MPa hydrogen pressure is shown in Fig. 6. The desorption kinetics persisted well, even after the 10th cycle, indicating that $HfCl_4$ is a good catalyst for the cycle life of MgH_2. The hydrogen storage capacity after 30 min desorption shows almost no decrease with cycling, being maintained at 6 wt.%, as shown in the inset of Fig. 6.

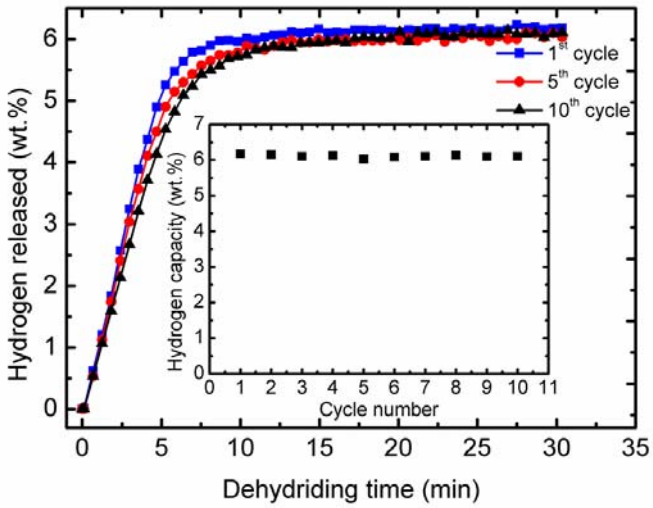

Fig. 6. The cycling performance of MgH_2 + 10 wt.% $HfCl_4$ at 300 °C under vacuum after rehydrogenation at 300 °C under 3 MPa hydrogen pressure. The main figure shows the hydrogen released in the 1st, 5th, and 10th cycles, while the inset shows the hydrogen capacity vs. cycle number.

Figs. 7 and 8 show XRD spectra for the $FeCl_3$ and $HfCl_4$-doped MgH_2 samples after milling, after dehydrogenation at 450 °C, and after rehydrogenation at 300 °C under 3 MPa hydrogen pressure. The results show that neither $FeCl_3$ nor $HfCl_4$, nor any secondary FeCl or HfCl-containing phase, was detected in either doped sample after milling, which is probably due to the

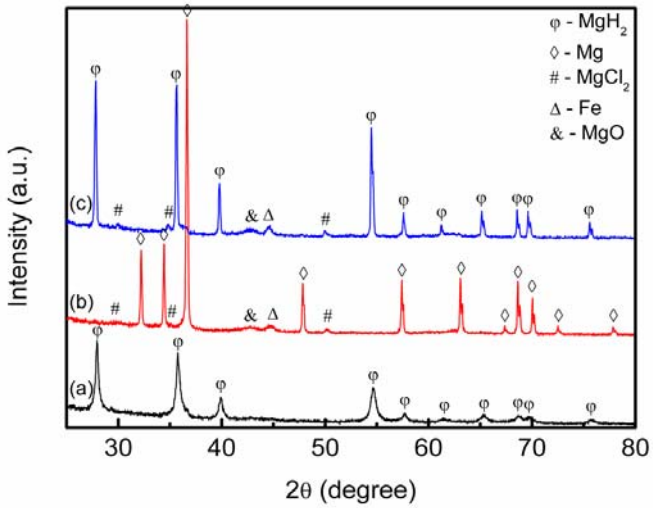

Fig. 7. X-ray diffraction patterns of the $FeCl_3$-doped MgH_2 (a) after milling, (b) after dehydrogenation, and (c) after rehydrogenation.

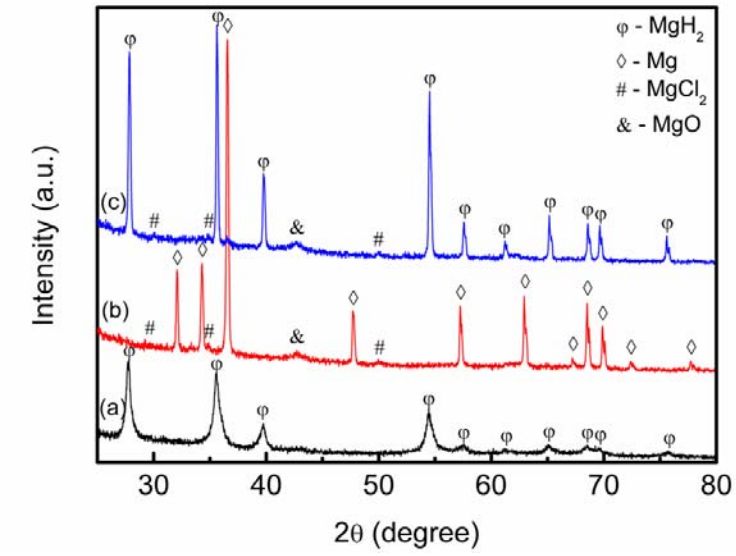

Fig. 8. X-ray diffraction patterns of the $HfCl_4$-doped MgH_2 (a) after milling, (b) after dehydrogenation, and (c) after rehydrogenation.

fact that the $FeCl_3$ and $HfCl_4$ grains are too small to be detectable in the MgH_2 matrix by XRD, or because the FeCl and HfCl-containing phases may exist in an amorphous state directly after ball milling. Theoretically, the reaction between MgH_2 and $HfCl_4$ or $FeCl_3$ may also occur during milling but they should not be easily detected in XRD due to fine crystalline or near-amorphous state incurred by high energy ball milling. In the dehydrogenation spectra for both samples, there are distinct peaks of Mg, which indicates that the reactions were completed. A small amount of MgO was also detected in the dehydrogenation spectra due to slight oxygen contamination. In addition, some peaks of $MgCl_2$ appear after dehydrogenation, suggesting that the reactions of MgH_2 + 10 wt.% $FeCl_3$ and MgH_2 + 10 wt.% $HfCl_4$ may occur as follows:

$$3MgH_2 + 2FeCl_3 \rightarrow 3MgCl_2 + 2Fe + 3H_2 \quad (2)$$

$$2MgH_2 + HfCl_4 \rightarrow 2MgCl_2 + Hf + 2H_2 \quad (3a)$$

or

$$2MgH_2 + HfCl_4 \rightarrow 2MgCl_2 + HfH_2 + H_2 \quad (3b)$$

For the $FeCl_3$-doped MgH_2 sample (Fig. 7b), peaks assigned to Fe are present, but no evidence of Hf-containing phase is observed for the $HfCl_4$-doped MgH_2 sample (Fig. 8b) after dehydrogenation. For the rehydrogenated sample, it can be seen that Mg is largely transformed into MgH_2. Peaks of $MgCl_2$ still remain, together with a small amount of MgO. For the $FeCl_3$-doped MgH_2 sample (Fig. 7c), Fe species still remain unchanged after rehydrogenation.

The effect of $FeCl_3$ and $HfCl_4$ addition on the MgH_2 bonding was investigated by FTIR measurements. The FTIR spectra for the as-milled MgH_2, the as-milled MgH_2 + 10 wt.% $FeCl_3$ and the as-milled MgH_2 + 10 wt.% $HfCl_4$ are shown in Fig. 9. According to Wang et al. [41], there are two main regions with active infrared vibrations of the Mg – H bonds, in which the spectra in the 400-800 cm^{-1} region correspond to the Mg – H bending bands and the spectra in the 900 – 1300 cm^{-1} region correspond to the Mg – H stretching bands. In our study, the stretching and bending bands for the as-milled MgH_2 are centred at about 1234 cm^{-1} and about 704 cm^{-1}, respectively. After doping with $FeCl_3$ and $HfCl_4$, hardly any difference was found in the FTIR spectra, indicating that the MgH_2 lattice is essentially unaffected by the presence of $HfCl_4$ and $FeCl_3$. Or, the changes are too small to be detected since the mole fraction of $HfCl_4$ and $FeCl_3$ are much smaller than that of MgH_2 and therefore the majority of MgH_2 just appears chemically intact in the FTIR results.

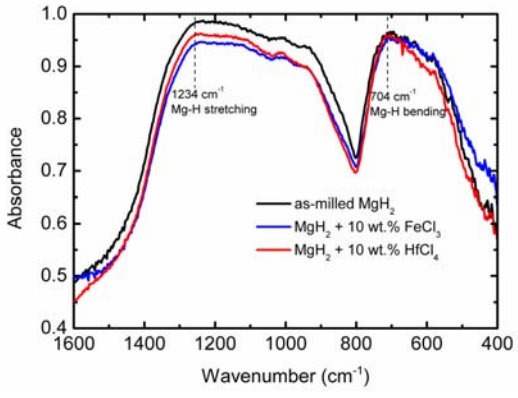

Fig. 9. FTIR spectra of as-milled MgH_2, MgH_2 + 10 wt.% $FeCl_3$, and MgH_2 + 10 wt.% $HfCl_4$.

As discussed above, the formation of $MgCl_2$ is probably due to the reaction between MgH_2 and $HfCl_4$ during the dehydrogenation process (Eq. 3(a) or (b)). The XRD spectra for the dehydrogenated and rehydrogenated samples show no detection of Hf-containing phases, due to their low concentration or amorphous structure. In order to investigate the nature of the Hf-containing species after dehydrogenation and after rehydrogenation in more detail, XPS measurements were conducted. Fig. 10 shows the Hf 4f spectra for pure $HfCl_4$ and for the $HfCl_4$-doped MgH_2 samples after dehydrogenation and after rehydrogenation. The pure $HfCl_4$ sample shows the characteristic peaks of Hf^{4+}, situated at 20.3663 eV for $4f_{5/2}$ and 18.6500 eV for $4f_{7/2}$, as shown in Fig. 10a.

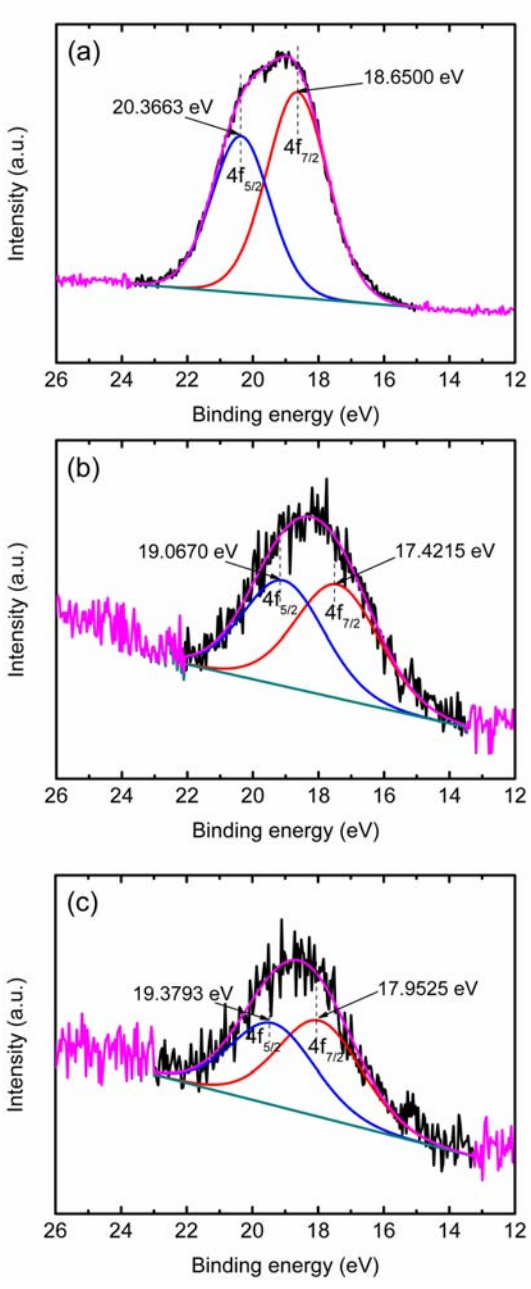

Fig. 10. XPS Hf 4f spectra with fitting results for pure $HfCl_4$ (a) and for MgH_2 + 10 wt.% $HfCl_4$ after (b) dehydrogenation and (c) rehydrogenation.

The Hf 4f transition was less pronounced in the $HfCl_4$-added MgH_2 samples than in the pure $HfCl_4$. In order to better identify the response from Hf in the spectra recorded for the $HfCl_4$-added MgH_2 sample after dehydrogenation and after rehydrogenation, *in situ* ion milling (for 10 min) using an Ar ion source with ion energy of 5 keV, as described in a previous paper [42], was employed. This resulted in a better signal-to-noise value for the Hf 4f peak as compared with that recorded for the same sample before the ion etching, although the noise level was still comparable with the signal.

Deconvolution of the peak structure using the CasaXPS2.3.15 software package was performed for the fitting of the peak structure obtained for the $HfCl_4$-added MgH_2 samples; Fig. 10b and 10c show the fitting results for the samples after dehydrogenation and after rehydrogenation. It is found that the dehydrogenation and rehydrogenation processes result in the shift of the Hf $4f_{5/2}$ and Hf $4f_{7/2}$ peaks from $HfCl_4$. For the sample after dehydrogenation, the position of the Hf $4f_{5/2}$ peak and of the Hf $4f_{7/2}$ peak is 19.0670 eV and 17.4215 eV, respectively. After rehydrogenation, there was no significant change in the Hf 4f transition that could be observed in our XPS measurements. (The positions of the Hf $4f_{5/2}$ and the Hf $4f_{7/2}$ peaks were 19.3793 eV and 17.9525 eV, respectively.) Due to the lack of evidence of local structure, we attribute these signals of intermediate valence states to Hf^{x+}-containing compounds ($0 < x < 4$).

In order to investigate the Hf-containing phase after dehydrogenation and after rehydrogenation in more detail, we prepared a MgH_2 sample with 50 wt.% $HfCl_4$, since it is not easy to analyse the phase composition of the sample with 10 wt.% $HfCl_4$ by XRD. Fig. 11 displays the XRD patterns of the MgH_2 sample with 50 wt.% $HfCl_4$ after 1 h of milling, after dehydrogenation at 450 °C, and after rehydrogenation at 300 °C under 3 MPa hydrogen pressure. After 1 h ball milling, only MgH_2 phase was detected, indicating that the $HfCl_4$ phase is in an amorphous state directly after ball milling. After dehydrogenation at 450 °C, as compared with the dehydrogenated MgH_2 + 10 wt.% $HfCl_4$ sample (Fig. 8(b)), a new diffraction peaks was formed, which is indexed as HfH_2. From the results, we assume that reaction 3(b) occurred during the dehydrogenation process in MgH_2 + 50 wt.% $HfCl_4$. According to Barraud et al. [43], grinding of hydrated hafnium tetrachloride, ph-$HfCl_4$ + Mg leads to the formation of hafnium hydride, and this hydride starts to decompose at about 500 °C. After rehydrogenation, this diffraction peaks still remain unchanged. Based on this result, it is likely that HfH_2 was also formed during the dehydrogenation process in the 10 wt.% $HfCl_4$-doped MgH_2 sample.

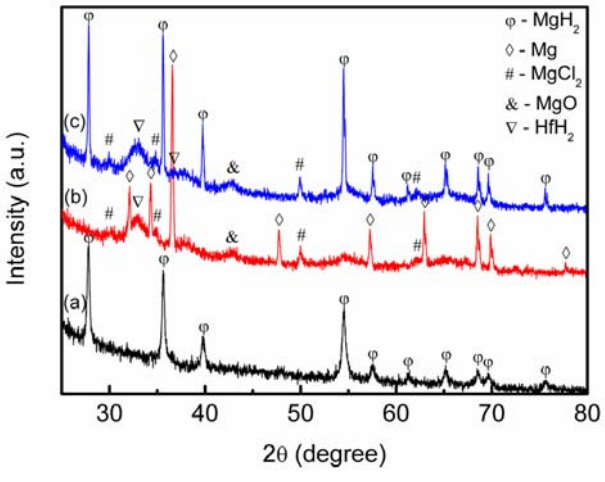

Fig. 11. X-ray diffraction patterns of the 50 wt.% $HfCl_4$-doped MgH_2 (a) after milling, (b) after dehydrogenation and (c) after rehydrogenation.

XRD examination of the dehydrogenated $FeCl_3$ and $HfCl_4$-doped MgH_2 samples identifies the formation of $MgCl_2$, and this product still remains after rehydrogenation. The formation of $MgCl_2$ encourages us to speculate that $MgCl_2$ may be acting as a real catalyst. In addition, we assume that Hf exist as a reaction product from reaction 3(a) during the dehydrogenation process. So, to examine the effects of $MgCl_2$ and Hf on MgH_2, samples of MgH_2 doped with 10 wt.% $MgCl_2$, Hf, and ($MgCl_2$ + Hf) were prepared, as shown in Fig. 12. For comparison, the as-milled MgH_2 and the MgH_2 + 10 wt.% $HfCl_4$ are also included in this figure. It is clear that the dehydrogenation temperature of MgH_2 was improved by doping with $MgCl_2$, ($MgCl_2$+Hf), and Hf compared to as-milled MgH_2.

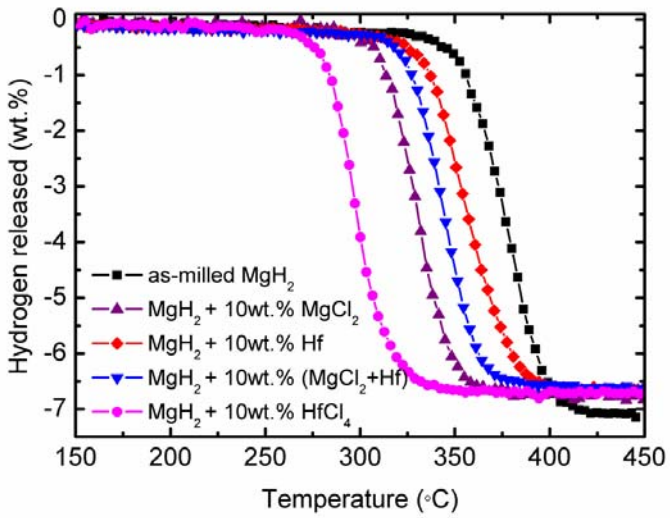

Fig. 12. Temperature-programmed desorption (TPD) patterns for the dehydrogenation of as-milled MgH_2, and MgH_2 doped with 10 wt.% $MgCl_2$, Hf, ($MgCl_2$+Hf), and $HfCl_4$.

Fig. 12 shows that $MgCl_2$, Hf, and ($MgCl_2$ + Hf) also have a positive influence on the hydrogenation behaviour of MgH_2, but it is not as good as that of MgH_2 + 10 wt.% $HfCl_4$. Therefore, Hf^{x+} - containing compound may act as the actual catalyst in the $HfCl_4$-doped MgH_2 system. Many studies have shown that transition metals act as catalysts in the dissociation of hydrogen molecules and the recombination of hydrogen atoms in the molecular state. A theoretical study of Nobuhara et al. [44] shows that, as hydrogen molecules reach the catalyst surface, charge is donated from the hydrogen s-orbitals to the surface s- and d-states, accompanied by a back donation from the surface s- and d-states to the hydrogen anti-bonding states. The interaction of the surface s- and d-electrons with hydrogen molecular orbitals enhances the hydrogen dissociation on the surfaces. During the desorption process, the Mg-H bond of MgH_2 is activated by the catalyst, so that the electrons of the bonding orbitals of MgH_2 are donated to the unoccupied orbitals of the catalyst, and subsequently, the electrons of the

occupied orbitals of the catalyst are back donated to the antibonding orbitals of the MgH_2 (back-donation) [45]. The electronic exchange reactions result in easier Mg-H dissociation, thus favouring the recombination of hydrogen atoms into hydrogen molecules. In this study, the valence electron configurations of Hf^{x+} are $6s^25d^{2-x}$, compared with $6s^25d^2$ for Hf. Clearly, the lower 5d orbital occupancy of Hf^{x+} allows an increased electron exchange with hydrogen molecules and Mg-H bonds of MgH_2. As a result, Hf^{x+}-species may have a more pronounced catalytic effect than metallic Hf, as supported by the TPD measurements presented in Fig. 12. Based on the XRD results of de/rehydrogenation of MgH_2 + 50 wt.% $HfCl_4$ (Fig. 11b and 11c), we speculate that the enhancement of sorption properties of the $HfCl_4$-doped MgH_2 sample may be due to the HfH_2 species. This speculation is in agreement with Kyoi et al. [46], who reported that a mixture of MgH_2 and HfH_2 heated up to 600°C under 4 – 8 GPa hydrogen in a multi-anvil cell showed an improved desorption temperature of MgH_2. In the case of the $FeCl_3$-doped MgH_2 sample, the formation of Fe during the dehydrogenation process may play an important role in enhancement of MgH_2 sorption, since it is well known that Fe is a good catalyst for MgH_2 [17, 47]. The presence of Fe metal may interact with hydrogen molecules, which may lead to the dissociation of hydrogen molecules and the improvement of the desorption/absorption rate.

Apart from the speculated catalytic effects of Fe and Hf species, the function of Cl^- may also introduce an extra catalytic effect on MgH_2 sorption properties. As shown in Fig. 12, $MgCl_2$ also has a positive influence on the dehydrogenation behaviour of MgH_2. The catalytic effect of $MgCl_2$ may further combine with the catalytic function of Fe or Hf species to generate a synergetic effect. However, further work is still required to clarify more details on the exact role of $HfCl_4$ and $FeCl_3$ addition in MgH_2.

4. Conclusion

This study shows that $HfCl_4$ and $FeCl_3$ are both effective additives for improving the dehydrogenation temperature and sorption kinetics of MgH_2. Both of the doped samples start to release hydrogen at about 270 °C, a decrease of about 70 °C and about 140 °C compared to the as-milled and as-received MgH_2, respectively. A hydrogen desorption capacity of 6.0 wt.% can be reached within 10 min at 300 °C for the $HfCl_4$-doped MgH_2 sample and 3.5 wt.% for the $FeCl_3$-doped MgH_2 sample, while only 0.2 wt.% hydrogen was desorbed by MgH_2. Meanwhile, 5.5 wt.% hydrogen was absorbed at 300 °C under 3 MPa hydrogen in 60 s for the $HfCl_4$-doped MgH_2 sample and 4.8 wt.% for the $FeCl_3$-doped MgH_2 sample, while the MgH_2 sample only absorbed 3.0 wt.% hydrogen under the same conditions. The apparent activation energy, E_A, for hydrogen desorption was estimated to be 102 kJ/mol and 130 kJ/mol for the $HfCl_4$-doped MgH_2 and the $FeCl_3$-doped MgH_2 samples, a decrease of 64 and 36 kJ/mol, respectively compared to the as-milled MgH_2 (166 kJ/mol). In addition, a cycling study of dehydrogenation at 300 °C showed that the hydrogen capacity of the $HfCl_4$-doped MgH_2 sample was maintained at about 6.0 wt.% after 10 cycles. From the XRD and XPS results, we suggest that the significant improvement in the MgH_2 sorption properties was due to the catalytic effect of Fe and Hf species that formed during the dehydrogenation process. In addition, the formation of $MgCl_2$ may also play a critical role, and it is very likely that there are synergetic effects, when $MgCl_2$ is combined with Fe and Hf species.

Acknowledgements

The authors thank the University of Wollongong for financial support of this research. M. Ismail acknowledges the Ministry of Higher Education Malaysia for a PhD scholarship. Many thanks also go to Dr. I. P. Nevirkovets for his help in XPS analysis and Dr. T. Silver for critical reading of the manuscript.

References

[1] Bhat VV, Contescu CI, Gallego NC, Baker FS. Atypical hydrogen uptake on chemically-activated, ultramicroporous carbon. Carbon 2010;48:1331-40.
[2] Zhao W, Fierro V, Zlotea C, Aylon E, Izquierdo MT, Latroche M, et al. Activated carbons with appropriate micropore size distribution for hydrogen adsorption. Int J Hydrogen Energy 2011;36:5431-4.
[3] Sakintuna B, Lamari-Darkrim F, Hirscher M. Metal hydride materials for solid hydrogen storage: A review. Int J Hydrogen Energy 2007;32:1121-40.
[4] Ismail M, Zhao Y, Yu XB, Dou SX. Improved hydrogen storage performance of MgH_2-$NaAlH_4$ composite by addition of TiF_3. Int J Hydrogen Energy 2012;37:8395-401.
[5] Ismail M, Zhao Y, Yu XB, Dou SX. Effects of NbF_5 addition on the hydrogen storage properties of $LiAlH_4$. Int J Hydrogen Energy 2010;35:2361-7.
[6] Ismail M, Zhao Y, Yu XB, Ranjbar A, Dou SX. Improved hydrogen desorption in lithium alanate by addition of SWCNT-metallic catalyst composite. Int J Hydrogen Energy 2011;36:3593-9.
[7] Mao J, Guo Z, Yu X, Ismail M, Liu H. Enhanced hydrogen storage performance of $LiAlH_4$-MgH_2-TiF_3 composite. Int J Hydrogen Energy 2011;36:5369-74.
[8] Zaluska A, Zaluski L, Ström-Olsen JO. Structure, catalysis and atomic reactions on the nano-scale: a systematic approach to metal hydrides for hydrogen storage. Appl Phys A 2001;72:157-65.
[9] Imamura H, Masanari K, Kusuhara M, Katsumoto H, Sumi T, Sakata Y. High hydrogen storage capacity of nanosized magnesium synthesized by high energy ball-milling. J Alloys Compd 2005;386:211-6.
[10] Zaluski L, Zaluska A, Ström-Olsen JO. Nanocrystalline metal hydrides. J Alloys Compd 1997;253-254:70-9.
[11] Zhu M, Wang H, Ouyang LZ, Zeng MQ. Composite structure and hydrogen storage properties in Mg-base alloys. Int J Hydrogen Energy 2006;31:251-7.
[12] Johnson SR, Anderson PA, Edwards PP, Gameson I, Prendergast JW, Al-Mamouri M, et al. Chemical activation of MgH_2; a new route to superior hydrogen storage materials. Chem Commun 2005;2823-5.
[13] Jin S-A, Shim J-H, Ahn J-P, Cho YW, Yi K-W. Improvement in hydrogen sorption kinetics of MgH_2 with Nb hydride catalyst. Acta Mater 2007;55:5073-9.
[14] Zaluska A, Zaluski L, Ström-Olsen JO. Nanocrystalline magnesium for hydrogen storage. J Alloys Compd 1999;288:217-25.
[15] Barkhordarian G, Klassen T, Bormann R. Effect of Nb_2O_5 content on hydrogen reaction kinetics of Mg. J Alloys Compd 2004;364:242-6.
[16] Gennari FC, Castro FJ, Urretavizcaya G, Meyer G. Catalytic effect of Ge on hydrogen desorption from MgH_2. J Alloys Compd 2002;334:277-84.
[17] Hanada N, Ichikawa T, Fujii H. Catalytic effect of nanoparticle 3d-transition metals on hydrogen storage properties in magnesium hydride MgH_2 prepared by mechanical milling. J Phys Chem B 2005;109:7188-94.
[18] Molinas B, Ghilarducci AA, Melnichuk M, Corso HL, Peretti HA, Agresti F, et al. Scaled-up production of a promising Mg-based hydride for hydrogen storage. Int J Hydrogen Energy 2009;34:4597-601.
[19] Croston DL, Grant DM, Walker GS. The catalytic effect of titanium oxide based additives on the dehydrogenation and hydrogenation of milled MgH_2. J Alloys Compd 2010;492:251-8.

[20] Hanada N, Ichikawa T, Isobe S, Nakagawa T, Tokoyoda K, Honma T, et al. X-ray absorption spectroscopic study on valence state and local atomic structure of transition metal oxides doped in MgH_2. J Phys Chem C 2009;113:13450-5.
[21] Ma LP, Kang XD, Dai HB, Liang Y, Fang ZZ, Wang PJ, et al. Superior catalytic effect of TiF_3 over $TiCl_3$ in improving the hydrogen sorption kinetics of MgH_2: Catalytic role of fluorine anion. Acta Mater 2009;57:2250-8.
[22] Luo Y, Wang P, Ma L-P, Cheng H-M. Hydrogen sorption kinetics of MgH_2 catalyzed with NbF_5. J Alloys Compd 2008;453:138-42.
[23] Zheng S, Fang F, Zhang J, Sun L, He B, Wei S, et al. Study of the Correlation between the Stability of Mg-Based Hydride and the Ti-Containing Agent. J Phys Chem C 2007;111:14021-5.
[24] Malka IE, Pisarek M, Czujko T, Bystrzycki J. A study of the ZrF_4, NbF_5, TaF_5, and $TiCl_3$ influences on the MgH_2 sorption properties. Int J Hydrogen Energy 2011;36:12909-17.
[25] Jin S-A, Shim J-H, Cho YW, Yi K-W. Dehydrogenation and hydrogenation characteristics of MgH_2 with transition metal fluorides. J Power Sources 2007;172:859-62.
[26] Mao J, Guo Z, Yu X, Liu H, Wu Z, Ni J. Enhanced hydrogen sorption properties of Ni and Co-catalyzed MgH_2. Int J Hydrogen Energy 2010;35:4569-75.
[27] Amirkhiz BS, Danaie M, Barnes M, Simard B, Mitlin D. Hydrogen Sorption Cycling Kinetic Stability and Microstructure of Single-Walled Carbon Nanotube (SWCNT) Magnesium Hydride (MgH_2) Nanocomposites. J Phys Chem C 2010;114:3265-75.
[28] Shang CX, Guo ZX. Effect of carbon on hydrogen desorption and absorption of mechanically milled MgH_2. J Power Sources 2004;129:73-80.
[29] Yu XB, Guo YH, Yang H, Wu Z, Grant DM, Walker GS. Improved Hydrogen Storage in Magnesium Hydride Catalyzed by Nanosized $Ti_{0.4}Cr_{0.15}Mn_{0.15}V_{0.3}$ Alloy. J Phys Chem C 2009;113:5324-8.
[30] Fan M-Q, Liu S-s, Zhang Y, Zhang J, Sun L-X, Xu F. Superior hydrogen storage properties of MgH_2-10 wt.% TiC composite. Energy 2010;35:3417-21.
[31] Wu C, Wang P, Yao X, Liu C, Chen D, Lu GQ, et al. Effects of SWNT and metallic catalyst on hydrogen absorption/desorption performance of MgH_2. J Phys Chem B 2005;109:22217-21.
[32] Luo Y, Wang P, Ma L-P, Cheng H-M. Enhanced hydrogen storage properties of MgH_2 co-catalyzed with NbF_5 and single-walled carbon nanotubes. Scripta Mater 2007;56:765-8.
[33] Ranjbar A, Ismail M, Guo ZP, Yu XB, Liu HK. Effects of CNTs on the hydrogen storage properties of MgH_2 and MgH_2-BCC composite. Int J Hydrogen Energy 2010;35:7821-6.
[34] Oelerich W, Klassen T, Bormann R. Metal oxides as catalysts for improved hydrogen sorption in nanocrystalline Mg-based materials. J Alloys Compd 2001;315:237-42.
[35] Shang CX, Bououdina M, Song Y, Guo ZX. Mechanical alloying and electronic simulations of (MgH_2+M) systems (M=Al, Ti, Fe, Ni, Cu and Nb) for hydrogen storage. Int J Hydrogen Energy 2004;29:73-80.
[36] Bobet JL, Akiba E, Nakamura Y, Darriet B. Study of Mg-M (M=Co, Ni and Fe) mixture elaborated by reactive mechanical alloying - hydrogen sorption properties. Int J Hydrogen Energy 2000;25:987-96.
[37] Xie L, Liu Y, Wang YT, Zheng J, Li XG. Superior hydrogen storage kinetics of MgH_2 nanoparticles doped with TiF_3. Acta Mater 2007;55:4585-91.
[38] Huot J, Liang G, Boily S, Van Neste A, Schulz R. Structural study and hydrogen sorption kinetics of ball-milled magnesium hydride. J Alloys Compd 1999;293-295:495-500.
[39] Ismail M, Zhao Y, Yu XB, Mao JF, Dou SX. The hydrogen storage properties and reaction mechanism of the MgH_2-$NaAlH_4$ composite system. Int J Hydrogen Energy 2011;36:9045-50.
[40] Ismail M, Zhao Y, Yu XB, Dou SX. Effect of different additives on the hydrogen storage properties of the MgH_2-$LiAlH_4$ destabilized system. RSC Advances 2011;1:408-14.
[41] Wang X, Andrews L. Infrared spectra of magnesium hydride molecules, complexes, and solid magnesium dihydride. J Phys Chem A 2004;108:11511-20.
[42] Ismail M, Zhao Y, Yu XB, Nevirkovets IP, Dou SX. Significantly improved dehydrogenation of $LiAlH_4$ catalysed with TiO_2 nanopowder. Int J Hydrogen Energy 2011;36:8327-34.

[43] Barraud E, Bégin-Colin S, Le Caër G, Barres O, Villieras F. Mechanically activated solid-state synthesis of hafnium carbide and hafnium nitride nanoparticles. J Alloys Compd 2008;456:224-33.
[44] Nobuhara K, Kasai H, Diño WA, Nakanishi H. H_2 dissociative adsorption on Mg, Ti, Ni, Pd and La Surfaces. Surf Sci 2004;566-568:703-7.
[45] Tsuda M, Diño WA, Kasai H, Nakanishi H, Aikawa H. Mg-H dissociation of magnesium hydride MgH_2 catalyzed by 3d transition metals. Thin Solid Films 2006;509:157-9.
[46] Kyoi D, Sakai T, Kitamura N, Ueda A, Tanase S. Synthesis of FCC Mg-Zr and Mg-Hf hydrides using GPa hydrogen pressure method and their hydrogen-desorption properties. J Alloys Comp 2008;463:311-6.
[47] Liang G, Huot J, Boily S, Van Neste A, Schulz R. Catalytic effect of transition metals on hydrogen sorption in nanocrystalline ball milled MgH_2-Tm (Tm=Ti, V, Mn, Fe and Ni) systems. J Alloys Comp 1999;292:247-52.